ASTROBIOLOGY
Volume 14, Number 3, 2014

DOI: 10.1089/ast.2013.1112

Controls on the Archean Climate System Investigated with a Global Climate Model

E.T. Wolf and O.B. Toon

Abstract

The most obvious means of resolving the faint young Sun paradox is to invoke large quantities of greenhouse gases, namely, CO_2 and CH_4. However, numerous changes to the Archean climate system have been suggested that may have yielded additional warming, thus easing the required greenhouse gas burden. Here, we use a three-dimensional climate model to examine some of the factors that controlled Archean climate. We examine changes to Earth's rotation rate, surface albedo, cloud properties, and total atmospheric pressure following proposals from the recent literature. While the effects of increased planetary rotation rate on surface temperature are insignificant, plausible changes to the surface albedo, cloud droplet number concentrations, and atmospheric nitrogen inventory may each impart global mean warming of 3–7 K. While none of these changes present a singular solution to the faint young Sun paradox, a combination can have a large impact on climate. Global mean surface temperatures at or above 288 K could easily have been maintained throughout the entirety of the Archean if plausible changes to clouds, surface albedo, and nitrogen content occurred. Key Words: Archean—Habitability—Atmosphere. Astrobiology 14, 241–253.

1. Introduction

Since the issue was first raised by Sagan and Mullen (1972), the faint young Sun paradox has remained a topic of curiosity for climate scientists, planetary scientists, and geologists alike. Geochemical indicators of paleo-ocean temperatures and greenhouse gas amounts hint at seemingly contradictory conditions during the Archean period of Earth's history spanning 3.8 to 2.5 billion years ago (Ga), a time when the Sun was only 75–82% as bright as today. Ocean temperatures during the Archean are believed to have been at least as warm as the present day and possibly warmer (Knauth and Lowe, 2003; Robert and Chaussidon, 2006; Hren *et al.,* 2009; Blake *et al.,* 2010). However, paleoatmospheric CO_2 concentrations were conventionally believed to have been too low to overcome the reduced luminosity of the young Sun without additional means of warming (Haqq-Misra *et al.,* 2008).

Recently, simulations in which general circulation models have been used show that only modest amounts of CO_2 may be needed to marginally rectify the paradox toward the end of the Archean. Wolf and Toon (2013) found that 0.015 bar of CO_2, the ''best guess'' estimate for atmospheric CO_2 during the late Archean provided by Driese *et al.* (2011), could have prevented Earth from freezing over during the late Archean (circa 2.8 Ga with 80% of the present day solar constant). However, global mean surface temperatures would have remained cold ($T_s = 270$ K), and the sea ice margin would have extended into midlatitudes (46°). This cool climate may be inconsistent with the lack of evidence for glaciation throughout the majority of the Archean (Feulner, 2012). With the addition of 10^{-3} bar of methane, surface temperatures and sea ice extent would have been nearly equal to those of present-day Earth ($T_s = 285$ K, sea ice margin at 68° latitude) (Wolf and Toon, 2013). Note also that the CO_2 partial pressure appropriate for the late Archean can be stretched higher than discussed here as Sheldon (2006) suggested ~ 0.025 bar as an upper limit. Thus, additional warming could possibly have occurred via conventional means (*i.e.,* greenhouse gases). CH_4 could feasibly have been higher than 10^{-3} bar as well. So long as the ratio of CH_4 to CO_2 remained less than about 0.1, photochemical hazes should not have formed (Haqq-Misra *et al.,* 2008; DeWitt *et al.,* 2009; Zerkle *et al.,* 2012). While photochemical hazes may have provided an effective ultraviolet shield for early Earth (Wolf and Toon, 2010), thick hazes may have had a strong cooling effect (Haqq-Misra *et al.,* 2008). Studies in which climate models of differing origin have been used have found similar greenhouse gas–to–surface temperature relationships for the Archean (Charnay *et al.,* 2013; Kunze *et al.,* 2013).

Department of Atmospheric and Oceanic Sciences, Laboratory for Atmospheric and Space Physics, University of Colorado, Boulder, Colorado.

However, outstanding questions remain. While solutions to the faint young Sun paradox with present-day surface temperatures or cooler may provide ample planetary surface area with moderate temperatures and open oceans, they fall short of the hot seawater temperatures indicated by some geochemical analyses of ancient marine sediments (Knauth and Lowe, 2003; Robert and Chaussidon, 2006). Granted, the hot seawater interpretation for the Archean climate is controversial (Jaffrés *et al.,* 2007; Shields and Kasting, 2007), and more recent estimates indicate seawater temperatures only slightly warmer than those in the present-day tropics (Hren *et al.,* 2009; Blake *et al.,* 2010). The faint young Sun paradox also becomes more severe as one probes deeper backward in time. At the onset of the Archean (circa 3.8 Ga), the Sun was only 75% as bright as today (Gough, 1981); thus more substantial warming is required to solve the paradox compared with the results presented by Haqq-Misra *et al.* (2008) and Wolf and Toon (2013), both of which consider the Sun at 80% of its present-day brightness. Of course, our confidence in geochemical indicators for both surface temperature and CO_2 become correspondingly weaker as one probes deeper back in time. Finally, evidence from banded iron formations suggests that atmospheric CO_2 during the Archean may be constrained to a mere 3 times the present atmospheric level (PAL) (Rosing *et al.,* 2010). This is considerably lower than CO_2 estimates derived from paleosols (Rye *et al.,* 1995; Hessler *et al.,* 2004; Sheldon, 2006; Driese *et al.,* 2011). However, again this interpretation of the banded iron formations remains controversial (Dauphas and Kasting, 2011; Reinhard and Planavsky, 2011). If either the requirement for hot surface temperatures, the climate of the earliest Archean, or the strict CO_2 constraint imposed by banded iron formations is considered, other mechanisms for warming the climate may still be needed to resolve the faint young Sun paradox.

The simulations presented by Wolf and Toon (2013) assume that, aside from the strength of the solar constant and atmospheric inventories of CO_2 and CH_4, the Archean Earth remained fundamentally similar to the present day. Model physics parameterizations are left in their default state, and the model reacts to changes in the shortwave and longwave radiative forcings only. However, other researchers have proposed systematic differences between the Archean and the present day that may have controlled early climate. Earth had a faster rotation rate in the distant past (Williams, 2000). This would have modulated atmospheric dynamics (Jenkins, 1996). Rosing *et al.* (2010) suggested that early Earth may have had fewer cloud condensation nuclei and significantly less emergent land; both would lower the planetary albedo. Goldblatt *et al.* (2009) suggested that early Earth may have had an increased inventory of atmospheric nitrogen that caused the sea level pressure to be greater than 1 bar. Increased pressures would broaden spectral lines and increase absorption from existing greenhouse species. In the present study, we tested these systematic changes to the Archean climate system, using a general circulation model. We first conducted a series of sensitivity tests, and we then combined warming mechanisms to find optimal warming scenarios for the duration of the Archean.

2. Methods

We used the Community Atmospheric Model version 3.0 (CAM3) from the National Center of Atmospheric Research (Collins *et al.,* 2004, 2006). The model used here is identical in construct to that used by Wolf and Toon (2013). Wolf and Toon (2013) provided an in-depth discussion of the base model, validations, and climate sensitivity tests for present-day and early Earth simulations. Here, we briefly outline the model configuration. The model uses $4° \times 5°$ horizontal resolution with 66 vertical levels reaching up to $\sim$90 km altitude. The model uses a mixed-layer ocean model and a thermodynamic sea ice model. Internal ocean energy terms are used to simulate ocean heat transport. Note that the ocean heat transport has been tuned to match the present day but varies as a function of the sea ice margin. The specific treatment of ocean heat transport and sea ice becomes increasingly important for simulations in which sea ice expands greatly relative to the present day. However, here we focus only on warm planets ($T_s \geq 288$ K) with little ice; thus our treatment of ocean heat transport and sea ice is not a critical factor. Clouds are treated by using bulk microphysical parameterizations for condensation, precipitation, and evaporation that control atmospheric water vapor, ice cloud condensate, and liquid cloud condensate fields (Rasch and Kristjánsson, 1998; Collins *et al.,* 2004). A correlated *k*-distribution radiative transfer package was implemented that is designed specifically for the high-CO_2, high-CH_4, anoxic conditions expected for the Archean (described in Wolf and Toon, 2013). All other model physics were left identical to the default settings except where described specifically in the following sections.

3. Sensitivity Tests of Warming Mechanisms

Sensitivity tests were conducted to isolate the warming gained from a variety of atmospheric conditions specific to the Archean and notably different from the present day. For a baseline case, we first simulated the late Archean time period with a solar constant of 1093.6 W m^{-2} (2.8 Ga, 80% of present day) warmed only by CO_2 and H_2O. Our baseline atmosphere consisted of 0.06 bar of CO_2, no methane, 0.00933 bar of argon gas, 0.9438 bar of N_2, and variable amounts of water vapor determined through self-consistent modeling of the hydrological cycle. Note that increasing N_2 above the PAL (0.79115 bar N_2) ensures that the mean sea level pressure is 1.013 bar, identical to the present day. The planetary rotation rate, cloud droplet number concentrations, cloud droplet sizes, and land properties were held identical to the present day. In this baseline simulation, the global mean surface temperature was 287.9 K, matching that of the present day [see Wolf and Toon (2013) Section 3.1 for an in-depth discussion of our baseline simulation]. In the following subsections, we consider plausible changes to the rotation rate, land surface albedo, cloud droplet properties, and total atmospheric pressure relative to our baseline simulation.

It should be noted that climate sensitivity is state-dependent (Hansen *et al.,* 2005; Caballero and Huber, 2013). Initial conditions affect the climate response to a given forcing. In particular, the surface temperature controls many factors of climate, including the distribution of snow cover, sea ice, water vapor, clouds, and ultimately the albedo and infrared opacity (via water vapor) of the planet. Our goal in this segment of the study was to test the sensitivity of climate to warming mechanisms starting from approximately present-

day temperatures. Climate sensitivities will likely deviate as one approaches tipping points such as a runaway greenhouse or a snowball Earth. However, a climate with surface temperatures near those of the present day may be centered between extremes of climate and upturns in climate sensitivity (Hansen *et al.,* 2005). Archean climates, under a weak Sun and warmed by thick greenhouses, tend to have slightly larger climate sensitivities than that of present-day Earth over a wide range of conditions (Wolf and Toon, 2013). Climate models of differing origin and construction also may yield varying climate responses (Bony *et al.,* 2006).

3.1. Rotation rate

The Earth–Moon orbital system can be treated as a closed system subject only to the force of gravity. Differential gravitational forces exerted by the Moon on Earth cause the oceans to bulge outward, creating oceanic tides. However, Earth's rotation drags the tidal bulge, placing it slightly ahead of the Earth–Moon axis. As the Moon pulls back on the slightly off-axis tidal bulge, it exerts a subtle torque on Earth counter to the direction of rotation. Since angular momentum of the Earth–Moon system is conserved, this process causes the Moon to gain energy at the expense of Earth. Earth's rotation rate is slowed, while the Moon moves farther from Earth. This process has been ongoing since the formation of the Earth–Moon system. Extrapolating backward in time, Earth must have had a faster rotation rate in the distant past. Analysis of sedimentary deposits within ancient tidal zones and analysis of the fossils of ancient marine invertebrates both indicate that the length of day was likely near 18 h during the late Archean (Williams, 2000; Denis *et al.,* 2002). However, other studies indicate that the length of day may have been as short as 14 h circa 4.0 Ga (Zahnle and Walker, 1987).

Jenkins (2000, 2001) found that the obliquity of early Earth may have played a strong role in controlling climate. High obliquity (70°) could produce relatively warm Archean climates with only a few thousand parts per million of CO_2 by changing the latitudinal distribution of solar insolation. However, it is unclear how Earth may have migrated to such an extreme obliquity and then back to its present 23.4° obliquity. For all simulations in this work, we assumed the present-day obliquity.

We conducted sensitivity tests of the Archean climate with day lengths of 15, 18, and 24 h. As expected from dynamical theory, a faster rotation rate caused the Hadley cells to become weaker and smaller in latitudinal extent. Zonal, meridional, and vertical motions all decreased in magnitude. It is well established that increasing rotation rates results in a decrease in poleward heat transport, allowing the tropics to stay warmer while cooling the poles (Hunt, 1979; Jenkins, 1996; Navarra and Boccaletti, 2002). As a result, the meridional temperature gradient steepens, but the effect is slight. For an 18 h day, zonal mean surface temperatures increased by ~1 K in the tropics while decreasing by ~3 K at the poles compared with a 24 h day. For a 15 h day, zonal mean surface temperatures increased by ~2 K in the tropics while decreasing by ~5 K at the poles (Fig. 1). Dynamical effects imparted subtle changes to the vertical and latitudinal structure of clouds; however, the effect on overall climate appears unimportant. Local differences in net cloud forcings can vary by $\pm 5\ W\ m^{-2}$ from our baseline case, but global mean net cloud forcings vary by less than $0.3\ W\ m^{-2}$ over the three rotation rate cases (Table 1). In total, with an 18 h day the global mean surface temperature rose by only a scant 0.2 K from our baseline simulation to reach 288.1 K. With a 15 h day, the global mean surface temperature rose 0.7 K to 288.6 K. Our findings largely confirm Jenkins (1996) work in which an earlier three-dimensional climate model was used. While identifiable changes to the climate system were found due to increased rotation rates, the overall warming gained was miniscule in the context of that needed to resolve the faint young Sun paradox.

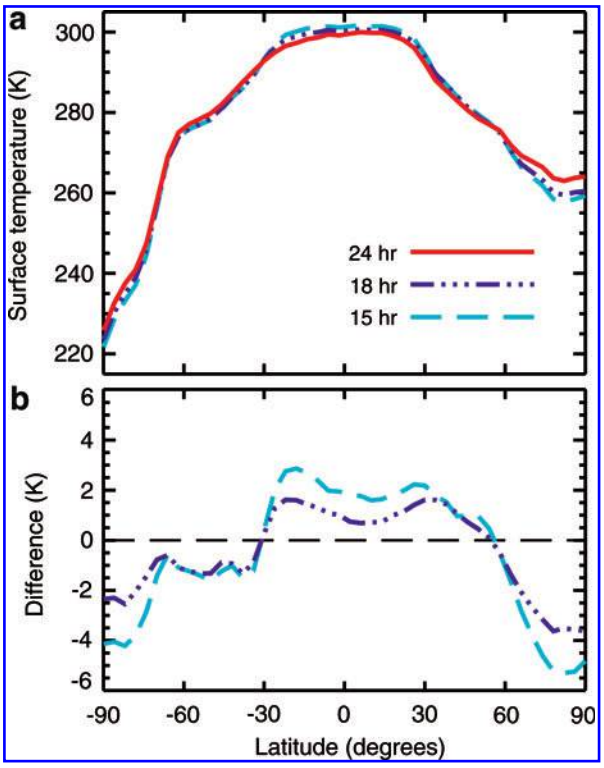

FIG. 1. Zonal and annual mean surface temperature (**a**) and the change in surface temperature (**b**) due to increased rotation rates. Increasing the rotation rate reduces meridional heat transports, thus steepening the meridional temperature gradient. However, global mean temperature differences are small (<1 K). (Color graphics available online at www.liebertonline.com/ast)

Using a three-dimensional ocean model coupled to a parameterized statistical atmosphere model, Kienert *et al.* (2012) found that increasing rotation rates leads to strong

TABLE 1. ROTATION RATE SENSITIVITY TESTS

Length of day (h)	24	18	15
Mean surface temperature (K)	287.9	288.1	288.6
Sea ice margin (degrees)	74.2	73.5	73.2
Cloud radiative forcing ($W\ m^{-2}$)			
Shortwave	−34.4	−34.6	−34.6
Longwave	25.3	25.5	25.8
Net	−9.1	−9.1	−8.8

cooling of the Archean, requiring 0.4 bar of CO_2 or more to overcome the faint young Sun. However, recent work with various general circulation models agrees well with our results presented here (Charnay *et al.,* 2013; Le Hir *et al.,* 2013). Increased rotation rates do not appear to play a significant role in warming the Archean.

3.2. Land surface albedo

Land surface albedo characteristics during the Archean were much different from today. Reductions to the planetary surface albedo have been proposed as at least a partial solution to the faint young Sun paradox (Rosing *et al.,* 2010). There was much less emergent continental crust during the Archean than there is today such that the Archean Earth would have been dominated by ocean (Dhuime *et al.,* 2012). What continents did exist were barren of vegetation. The earliest Archean continents were likely formed from dark basalts. As the continents aged, the surface texture may have changed into lighter-colored soils typical of modern-day desert regions (Rosing *et al.,* 2010). Presently, permanent land glaciers in Greenland, Antarctica, and mountainous regions add considerably to the surface albedo. Such semipermanent, land-based ice structures may have been absent from early Earth.

Here, we removed all surface vegetation and all continental ice sheets and tested ''light'' and ''dark'' bare soil surface configurations specified onto the present-day continental areas. Note that sea ice and snow cover were still permitted, both of which strongly modulate the surface albedo. For simplicity, we did not move or eliminate continental area and instead focused only on changes to land albedo. The albedo of bare soil depends upon moisture content and crudely upon wavelength (visible or near-infrared, demarcated at 0.7 μm). For light-colored soils, the water-saturated soil albedo in the visible (near-infrared) is 0.12 (0.24), while the dry albedo is 0.24 (0.48). For dark-colored soils, the water-saturated soil albedo in the visible (near-infrared) is 0.05 (0.10), while the dry albedo is 0.10 (0.20). The albedo of ocean is 0.06 across both the visible and near-infrared; thus the albedo of saturated dark soil approaches that of ocean.

Changing the albedo of the land had a limited effect on overall climate, as continental area constitutes only $\sim$30% of the total planetary surface. For our light (dark) simulation, the global mean surface albedo was 0.143 (0.105), while for our baseline simulation it was 0.136 (Table 2). Note that the baseline model has a slightly lower overall surface albedo than light soil. Modest gains in global mean surface temperature were found for both light and dark soil simulations compared with our baseline case. The dark soil global mean surface temperature rose 3.7 K to 291.6 K, while exhibiting a 23% percent decrease in the global mean surface albedo compared with the baseline simulation. The light soil global mean surface temperature rose 0.9 K to 288.8 K despite having a slightly larger global mean surface albedo than the baseline case. This can be attributed to two factors: reduced low cloud fractions ($p > 700$ mb) over land and significantly decreased surface albedos over the Antarctic continent and Greenland.

Replacing all forested and vegetated land areas with bare soil resulted in a lower latent heat flux to the atmosphere because precipitation is more readily lost to runoff. In particular, tropical forested areas tend to hold water in the near-surface environment, allowing water to be cycled more easily back into the atmosphere, creating clouds in the lowest model layers. Thus by removing all surface vegetation (thereby creating a desert land type), we found a reduction in low clouds and a modest reduction to the magnitude of shortwave cloud forcings (Table 2). This effect became less pronounced for the dark soil simulation because increasing global air temperatures enhanced ocean surface evaporation rates, allowing more moisture into the atmosphere.

Table 2. Surface Albedo Sensitivity Tests

Soil surface configuration	Present day	Light	Dark
Mean surface temperature (K)	287.9	288.8	291.6
Sea ice margin (degrees)	74.2	75.6	77.9
Surface albedo	0.136	0.143	0.105
Cloud fraction			
Low	0.309	0.293	0.296
Middle	0.233	0.214	0.232
High	0.540	0.548	0.541
Cloud radiative forcing ($W\,m^{-2}$)			
Shortwave	−34.4	−31.9	−33.9
Longwave	25.4	25.6	25.9
Net	−9.0	−6.3	−8.0

Reduced surface albedos in the polar regions exist due to the removal of semipermanent ice sheets. While large surface albedos are still found over the poles due to the accumulation of snow and the growth of sea ice, they remain slightly less than those found in our baseline simulation (Fig. 2b). In the model, periodic melts of snowpack over Antarctica and Greenland revealed a low-albedo soil surface instead of glacial ice (which was removed from the model in these simulations). Overall warmer climates found in both light and dark soil simulations ensure that sea ice distributions are reduced, further lowering polar surface albedos. Changes to the surface albedo and surface temperature are more pronounced in the northern hemisphere since this is where the majority of the continental area resides in our model (Fig. 2a).

Our results are in general agreement with recent analysis of the effect of land albedo on Archean climate (Goldblatt and Zahnle, 2011; Charnay *et al.,* 2013; Kunze *et al.,* 2013). Reducing the surface albedo results in a non-negligible gain in global mean temperature and may constitute a minor contributor toward warming early Earth. However, a solution to the faint young Sun paradox cannot rely on warming from a reduced surface albedo alone.

3.3. Clouds

Alternative solutions to the faint young Sun paradox have been proposed based on fundamental changes to cloud properties on early Earth. Notably, early Earth likely had fewer cloud condensation nuclei (CCN) (Andreae, 2007; Rosing *et al.,* 2010). CCN are important because at typical tropospheric temperatures water vapor requires the presence of aerosols to seed condensation and form cloud droplets. Where CCN are plentiful, cloud droplets tend to be more

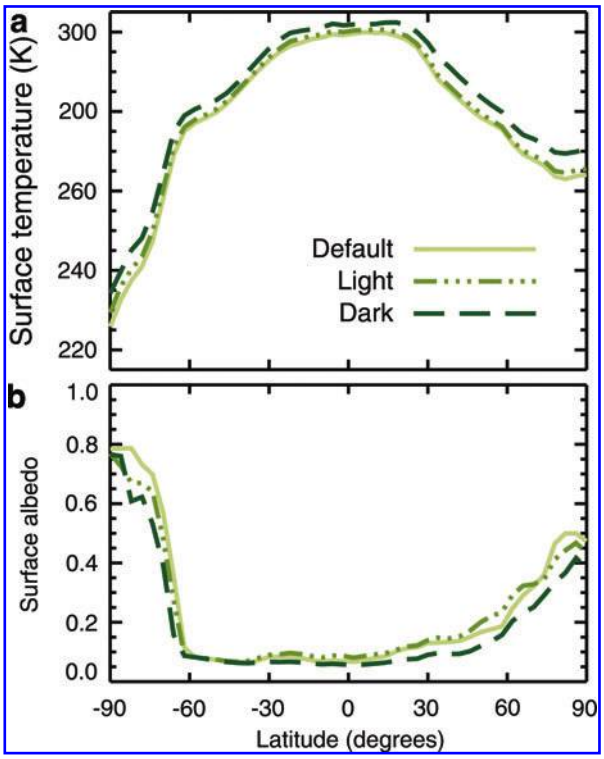

FIG. 2. Zonal and annual mean surface temperature (**a**) and surface albedo (**b**) for default, light, and dark land surface configurations. The mean surface temperature is affected both by changing the specified surface albedo and through a modest positive cloud forcing that occurs when removing forested land types in favor of bare soil (*i.e.,* desert). (Color graphics available online at www.liebertonline.com/ast)

numerous but smaller in size, creating clouds that are more reflective and have longer lifetimes against removal (via precipitation). Where CCN are few, cloud droplets are sparse but grow larger in size, creating clouds that are less reflective and rain out more quickly (Kump and Pollard, 2008). Thus, a reduction to cloud albedos driven by reductions to CCN concentrations may have provided a substantial warming mechanism for early Earth (Rosing *et al.,* 2010). At present, CCN are dominantly sourced by sea salt, dust, industrial pollution, biomass burning, and the oxidation of biologically produced compounds. The present-day CCN burden may be $\sim$100s cm^{-3} over biologically productive regions of the ocean, while possibly reaching 1000 cm^{-3} or more over active continental areas (Andreae, 2007). While the Archean obviously lacked anthropogenic pollutants, it was also anoxic and had much sparser biological activity than today. Archean life was primarily microbial and had not yet colonized the land (Schopf, 2006). Thus, one might expect that sea salt and dust were the only available CCN for early Earth.

Sea salt aerosols are produced as winds loft particles off whitecaps in turbulent oceans. Detailed three-dimensional modeling of sea salt CCN concentrations, supported by observations, predict values between 10 and 50 cm^{-3} over most of the world's oceans. In isolated regions of persistent high wind speeds (such as the ''roaring 40s'' on present Earth), sea salt CCN concentrations may approach 100 cm^{-3} (Fan and Toon, 2011). Early Earth would have had less continental area, so there may have been more surface area uninterrupted by land, promoting stronger zonal mean winds. However, this effect would have been offset by weakened overall circulation due to increased rotation rates. Presently, CCN found over biologically and photochemically inactive ocean regions are primarily sea salts, numbering only $\sim$10s cm^{-3} (Andreae, 2007). Similar conditions would likely have existed during the Archean.

Dust serves as CCN predominantly over desert regions; however, it is likely that all emergent continental crust was desertified and thus dusty. At present, over inland deserts dust may constitute up to 40% of the total CCN concentration and create 23.8% of the cloud droplet number concentration (CDNC) (Karydis *et al.,* 2011). This equates to local maximum values of CDNC sourced by dust to between 40 and 100 cm^{-3}; however, regional and global average values are much lower (Karydis *et al.,* 2011). Pre-industrial CCN concentrations over the continents are believed to have been between 50 and 200 cm^{-3} (Andreae, 2007); however, this estimate includes the contribution of biologically sourced CCN that would have been absent over Archean continents. Archean CCN concentrations over land were probably much lower than pre-industrial estimates.

CAM3 utilizes bulk parameterizations that determine the exchange between water vapor, cloud condensate, and precipitate (Rasch and Kristjánsson, 1998; Zhang *et al.,* 2003). Cloud condensate amounts are controlled by dynamical and thermodynamical processes; however, liquid CDNC and liquid cloud droplet effective radii are specified parameters rather than following from a self-consistent calculation based on the activation of CCN. CCN and CDNC are both closely related to the atmospheric aerosol burden, with CDNC by definition numbering less than the CCN burden (Karydis *et al.,* 2011; Hegg *et al.,* 2012). Note that the model treats ice and liquid cloud types with fundamentally different parameterizations. Ice cloud properties are determined by temperature and condensate mixing ratio alone and do not rely on fixed parameters for CDNC and effective radius (Kristjánsson and Kristiansen, 2000).

In the default setting, appropriate for present-day Earth, liquid CDNC are taken to be 400 cm^{-3} over land, 150 cm^{-3} over ocean, and 75 cm^{-3} over ice. We performed simulations with 50%, 20%, and 10% of default present-day CDNC, scaled evenly across land, ocean, and sea ice values (Table 3). For a given amount of cloud condensate, the cloud droplet effective radius varies as $CDNC^{-1/3}$. In the default setting, liquid cloud droplets achieve their maximum size of 14 μm over ocean and sea ice, while for our test simulations with reduced CDNC, cloud droplet maximum sizes found over ocean can be 17.6, 23.9, and 30.2 μm, respectively. Liquid cloud droplet sizes are slightly smaller over land owing to a larger aerosol burden (and thus more numerous CCN and CDNC). Rosing *et al.* (2010) suggested that cloud droplet sizes of 20 and 30 μm may be appropriate for the Archean. For reference, presently liquid cloud droplet sizes are observed to reach 17 μm over unproductive oceans far from human activities (Bréon *et al.,* 2002). Both liquid and ice cloud optical properties are determined by Mie scattering coefficients calculated at the cloud droplet effective radii.

Increasing liquid cloud droplet sizes has a twofold effect on climate. Clouds that consist of larger, but less numerous, droplets are inherently less reflective. Cloud droplet

Table 3. CDNC Sensitivity Tests

CDNC configuration	100% (default)	50%	20%	10%
Mean surface temperature (K)	287.9	291.2	294.6	296.6
Sea ice margin (degrees)	74.2	78.2	80.6	82.0
CDNC (# cm^{-3})				
Land	400	200	80	40
Ocean	150	75	30	15
Sea ice	75	37.5	15	7.5
Cloud droplet radii (μm)				
Land	8	10.1	13.7	17.2
Ocean	14	17.6	23.9	30.2
Sea ice	14	17.6	23.9	30.2
Cloud albedo	0.134	0.117	0.095	0.082
Water column ($kg\,m^{-2}$)				
Water vapor	20.2	24.4	30.5	34.6
Cloud liquid water	0.086	0.077	0.065	0.059
Cloud ice water	0.017	0.015	0.013	0.012
Cloud radiative forcing ($W\,m^{-2}$)				
Shortwave	−34.4	−30.2	−24.8	−21.5
Longwave	25.4	25.8	25.4	25.4
Net	−9.0	−4.4	0.6	3.9

extinction efficiencies are ~2 across visible and infrared wavelengths for all effective radii of interest here. Thus, for a given cloud water path, the cloud optical depth is inversely proportional to effective radius. Secondly, larger cloud droplets will more easily precipitate out of the atmosphere; thus total cloud water paths will be reduced. CAM3 parameterizes the conversion of liquid cloud condensate to rain following the method suggested by Chen and Cotton (1987). The rate of conversion of liquid cloud condensate to precipitate is proportional to the cloud droplet effective radius. However, other parameterizations use precipitate conversion rates as large as $R^{5.37}$ (as opposed to R^1 in this study), resulting in much more efficient rainout, fewer clouds, and more surface warming than is found here (Kump and Pollard, 2008; Charnay *et al.,* 2013).

Figure 3 shows the zonal mean cloud condensate mixing ratio (g/kg_{air}), including both ice and liquid for all four cloud simulations (default, 50%, 20%, 10%). Note that liquid cloud condensate dominates over ice condensate by a ratio of 5:1. For each successive reduction in CDNC, cloud condensate amounts fall. As cloud decks become thinner, the climate warms as expected. As CDNC are reduced, low (>700 mb) and mid (700–400 mb) level cloud fractions are reduced at middle and high latitudes but remain roughly equal over the tropics (Fig. 3, Fig. 4b, 4c). Note that the Archean had inherently fewer convective clouds due to weak solar insolation (Wolf and Toon, 2013). The magnitude of shortwave cloud forcings is strongly reduced at midlatitudes, by up to ~33 $W\,m^{-2}$ in the southern hemisphere and ~20 $W\,m^{-2}$ in the northern hemisphere for the 10% CDNC simulation compared with the default (Fig. 4e). Changes to cloud forcings are less over the tropics (~7 $W\,m^{-2}$ reduction in magnitude). On global mean, shortwave cloud forcings are reduced in magnitude by 12.9 $W\,m^{-2}$ for the 10% CDNC simulation compared with the default (Table 3). High-altitude (<400 mb) cloud fractions are reduced over the tropics; however, they are increased over high latitudes (Fig. 4a). This behavior is a feature of warming climates and is associated with polar amplification. It is not caused by our specified changes to liquid CDNC and liquid cloud droplet sizes. Similar behavior is observed in simulations that rely only on greenhouse gas warming with no alterations made to the default cloud parameterizations (not shown). There is little change to the longwave cloud forcings (Fig. 4d). Longwave cloud forcings are imparted most strongly by high-altitude ice clouds. In this set of simulations, ice cloud particles have not been altered; thus we would not expect to find significant changes here.

Simulations of present-day Earth using CAM3 indicate that clouds have a net radiative forcing of −24.9 $W\,m^{-2}$ and thus impart a strong cooling influence on climate (see also

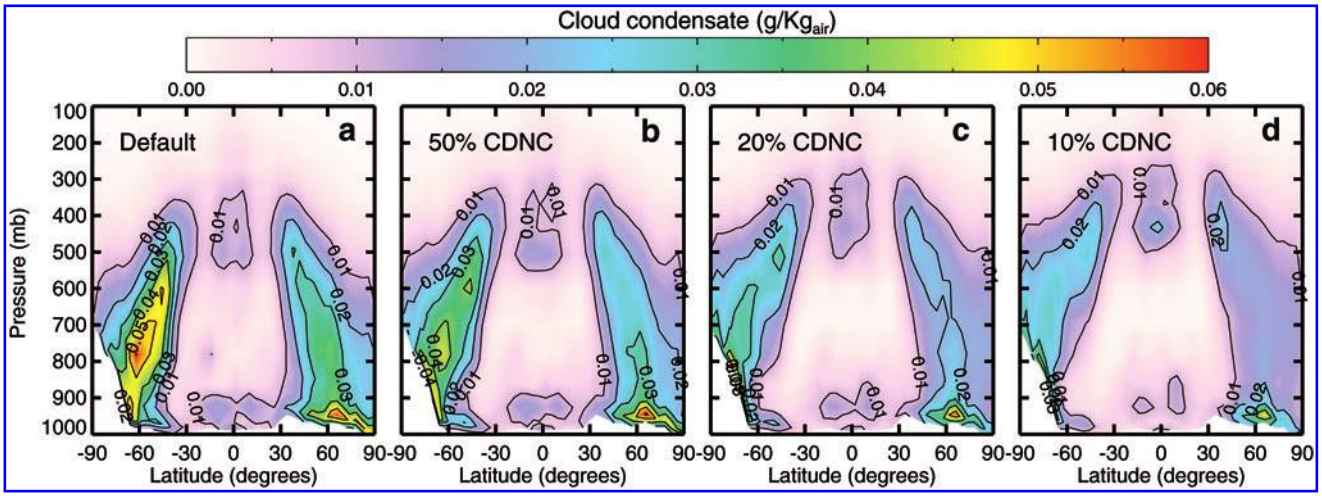

FIG. 3. Zonal and annual mean cloud condensate amounts from simulations with the default CDNC (**a**), 50% (**b**), 20% (**c**), and 10% (**d**) of the default values (see Table 3). Cloud condensate drops significantly as CDNC is reduced because cloud droplets are larger and thus rain out more efficiently. (Color graphics available online at www.liebertonline.com/ast)

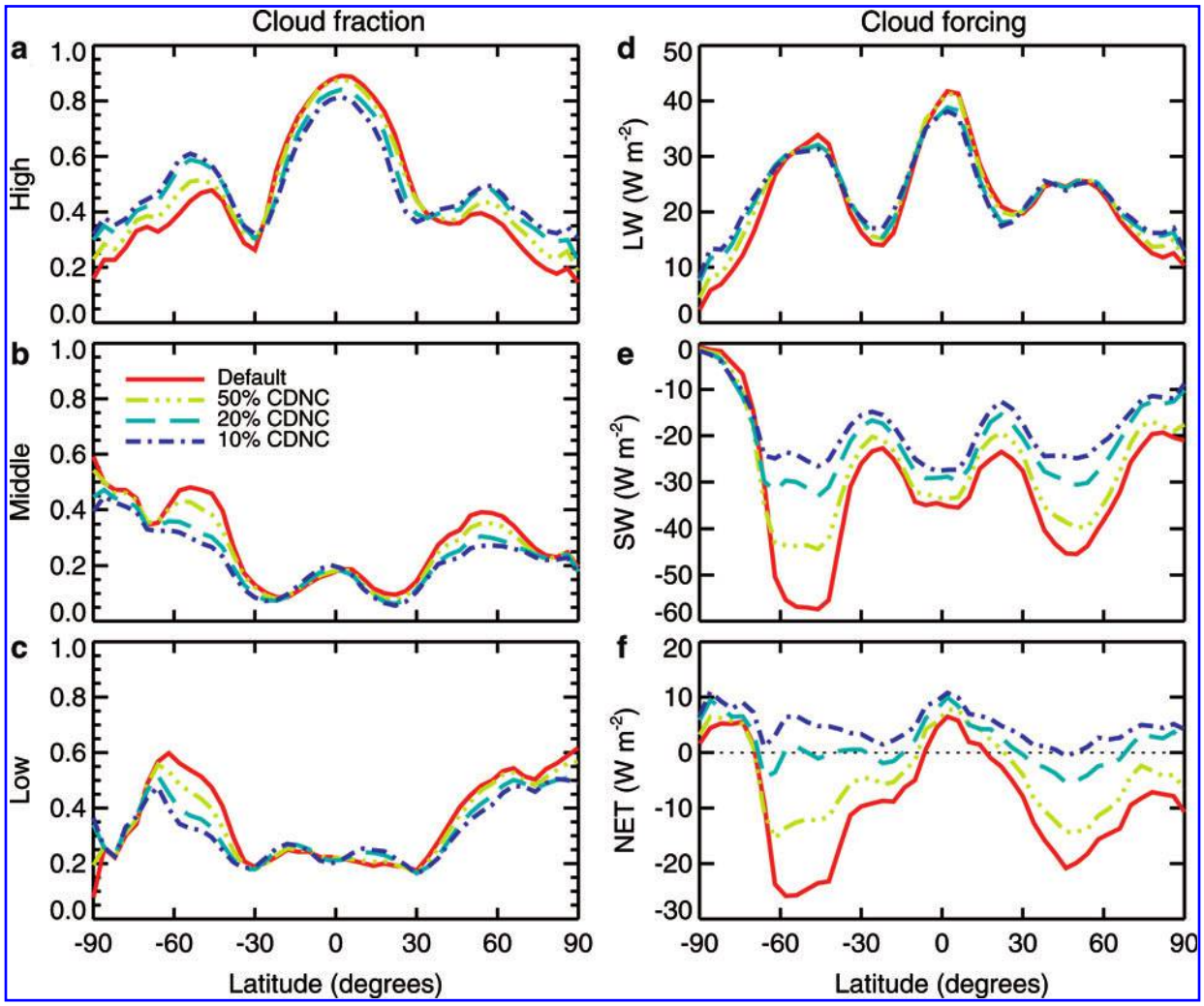

FIG. 4. Zonal and annual mean cloud fractions and cloud forcings for simulations with varying CDNC. Low cloud fractions ($p > 700$ mb) (**c**) and middle cloud fractions ($700 > p > 400$ mb) (**b**) both see significant reductions over midlatitudes as CDNC is decreased. High cloud fractions ($p < 400$ mb) (**a**) decrease over the tropics and increase over the poles. However, this feature is caused by overall warming to the planet along with polar amplification and is not affected by our choice of CDNC. Longwave cloud forcings (**d**) do not change significantly; however, the magnitude of shortwave cloud forcings (**e**) are greatly reduced, particularly over the midlatitudes. As CDNC is decreased, the net cloud forcing (**f**) grow less negative; thus the cooling effect of clouds is greatly weakened. (Color graphics available online at www.liebertonline.com/ast)

Collins *et al.,* 2006). For our baseline simulation of the late Archean in which default CDNC and cloud droplet sizes were used, clouds had a net radiative forcing of only $-9.0\,\mathrm{W\ m^{-2}}$ [see discussion in Wolf and Toon (2013) Section 3.1]. For simulations with 20% and 10% CDNC, global mean net cloud forcings became positive with values of $+0.6$ and $+3.9\,\mathrm{W\ m^{-2}}$, respectively (Table 3). With 10% CDNC, cloud net radiative forcings were positive virtually everywhere on the planet (Fig. 4f). Reducing CDNC to 10% had the largest effect on climate, increasing global mean surface temperatures by 8.7 K, reaching 296.6 K. Thus, while perhaps not a full solution to the faint young Sun paradox in its own right, reduced CCN (and thus reduced CDNC) during the Archean may have provided a fairly sizeable boost to surface temperatures. Even given our maximum change in net cloud forcing found to be $+12.9\,\mathrm{W\ m^{-2}}$ for our 10% CDNC case, our results fall within the ''plausible'' scenarios outlined by Goldblatt and Zahnle (2011).

It has also been proposed that feedbacks involving increased high-altitude (ice) clouds may have helped warm early Earth (Rossow *et al.,* 1982; Rondanelli and Lindzen, 2010). Due to their low radiating temperatures, high-altitude clouds can contribute strongly to the greenhouse effect. Very cold temperatures are found aloft in our Archean simulations, with minimum temperatures near 150 K, due to the absence of an ozone layer and increased radiative cooling from high CO_2 concentrations (Wolf and Toon, 2013). The model diagnoses large cloud fractions located near the deep atmospheric temperature minimum found at 1 mb ($\sim$30 km) (Fig. 5). Exceedingly low ambient temperatures cause very low saturation vapor pressures. Thus, high relative humidities are easily achieved, and large cloud fractions are found. While cloud ice water mixing ratios found here are much larger for Archean simulations compared with the present day ($\sim 10^{-8}$ versus $\sim 10^{-18}$, really there are no clouds in most of the present-day stratosphere, only over Antarctica in

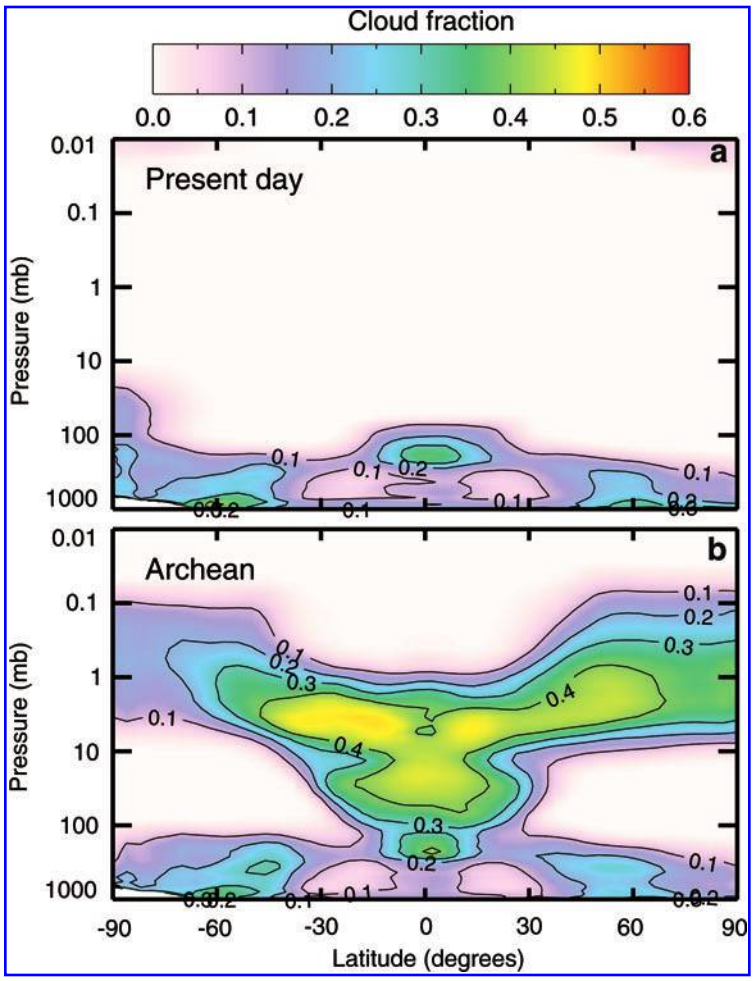

FIG. 5. Zonal and annual mean cloud fractions for present-day simulations (**a**) and for Archean simulations (**b**). The removal of ozone allows the Archean stratosphere to become very cold. Large cloud fractions are diagnosed in the Archean stratosphere because the saturation vapor pressure is quite low. Only a small amount of water vapor is needed to saturate the Archean stratosphere and cause ice particles to condense. (Color graphics available online at www.liebertonline.com/ast)

the polar night), they remain 2 orders of magnitude lower than typical cloud ice water mixing ratios found in the upper troposphere ($\sim 10^{-6}$).

It is unclear how ice particles might be systematically different during the Archean compared with the present day. Ice particle growth is primarily controlled by temperature because the amount of available water vapor is limited by temperature. Ice particle sizes increase monotonically with temperature (Kristjánsson and Kristiansen, 2000). In our baseline Archean simulation, ice particles in the upper ice cloud deck have sizes of ~ 0.5 μm near 1 mb pressures. Here, we have explored tuning the upper-level ice cloud deck based on the work of Urata and Toon (2013) in studying warm early martian climates. We conducted simulations where ice clouds above the tropopause were artificially forced to have larger particle sizes (10, 50, 100 μm) and 100% cloud fractions across the whole sky. However, these simulations failed to yield discernable warming. The upper cloud deck found in Archean simulations contains too little cloud water to have a significant impact on climate even when tuned to optimize the cloud greenhouse effect.

3.4. Atmospheric N_2 inventory

An accounting of Earth's nitrogen budget suggests that the total inventory of nitrogen existent on Earth, including both in the atmosphere and in the solid Earth, may total $14.8 \pm 5.3 \times 10^{18}$ kg. This is equal to 3 PAL N_2 as a best guess and 5 PAL as an upper limit (Goldblatt *et al.,* 2009). Low biological productivity during the Archean would have reduced the rate of nitrogen removal from the atmosphere via fixation and burial within sediments. Coupled with increased outgassing of nitrogen trapped in the mantle, the Archean biogeological system could have favored higher atmospheric N_2 inventories (Goldblatt *et al.,* 2009). Increasing the nitrogen content (and thus the total pressure) of the young atmosphere results in increased molecular absorption from existing greenhouse species through the pressure broadening of spectral lines. Som *et al.* (2012) attempted to constrain the surface air pressure of the late Archean by analyzing the imprints left from ancient raindrops in the 2.7 Ga Ventersdorp Supergroup, South Africa. Their most probable estimate places surface air pressure between 0.527 and 1.115 bar; thus the atmospheric nitrogen content was not likely much different than that of today (in fact, their estimate implies possibly reduced surface air pressures compared with the present day). However, their absolute upper limit on surface pressure is 2.128 bar, leaving open the possibility that the atmospheric nitrogen content was indeed much larger than that of the present day. Marty *et al.* (2013) constrained N_2 in the early atmosphere through an analysis of the $N_2/^{36}Ar$ ratios in fluid inclusions trapped in Archean quartz. Marty *et al.* (2013) concluded that the total surface pressure at 3.5 Ga was no more than 1.1 bar and

Table 4. Nitrogen Sensitivity Tests

pN_2 (PAL)	1	1.19	1.5	2	3
Sea level pressure (bar)	0.861	1.013	1.256	1.651	2.443
Mean surface temperature (K)	286.1	287.9	289.9	292.9	297.6
Sea ice margin (degrees)	71.3	74.2	77.3	80.6	86.8
Water column (kg m^{-2})					
Water vapor	18.8	20.2	22.0	24.6	30.8
Cloud liquid water	0.081	0.086	0.091	0.094	0.091
Cloud ice water	0.016	0.017	0.018	0.019	0.020
Cloud radiative forcing (W m^{-2})					
Shortwave	−34.3	−34.4	−34.4	−33.8	−31.1
Longwave	25.3	25.3	25.6	26.1	26.2
Net	−9.0	−9.1	−8.8	−7.7	−4.9

possibly as low as 0.5 bar. Nonetheless, given the overall low confidence in ancient geochemical indicators, here we will explore the idea of increased atmospheric N_2 as originally proposed by Goldblatt *et al.* (2009).

In the present study, we simulated atmospheres that have 1, 1.5, 2, and 3 PAL N_2 in addition to our baseline simulation (Table 4). Note that 1 PAL of N_2 is equal to 0.79115 bar. Our baseline simulation achieved a mean sea level pressure of 1.013 bar (identical to the present day) by invoking a slightly larger atmospheric N_2 inventory (~1.19 PAL N_2) to make up for the removal of oxygen. While increasing N_2 in the atmosphere enhanced the greenhouse forcing imparted by a static amount of the greenhouse gases, it also increased Rayleigh scattering (Fig. 6). However, the positive longwave forcing from the pressure broadening effect outpaced the negative shortwave forcing from enhanced scattering to space. Increasing surface temperatures and increasing surface pressures had competing effects on the hydrological cycle. Warming surface temperatures increased convection and thus increased clouds, both tending to cool to the surface. However, increasing surface pressure increased the absolute value of the moist adiabatic lapse rate, thus decreasing the frequency of convective instabilities and thinning cloud cover, both tending to warm the surface (Goldblatt *et al.,* 2009). These feedbacks partially offset. Here, we found modest reductions to the magnitude of shortwave cloud forcings as the surface pressure was increased. The strongest effect was found in the 3 PAL N_2 simulation, where the magnitude of the global mean shortwave cloud forcing was reduced by 3.3 W m^{-2}. Simulations with increased surface pressure also showed a small increase in the cloud greenhouse effect. Steeper lapse rates resulted in cold temperatures and larger relative humidities in the upper troposphere, causing a greater incidence of high ice clouds. However, this effect on climate remained small, contributing <1 W m^{-2} of additional forcing to the cloud greenhouse effect.

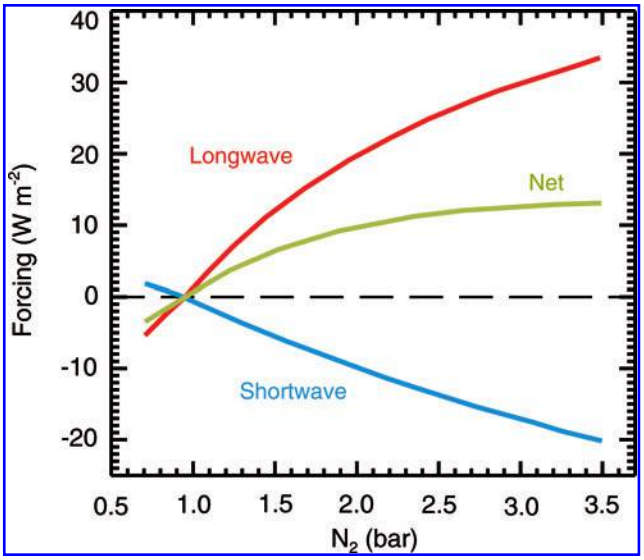

FIG. 6. Global mean instantaneous clear sky radiative forcing from increasing the nitrogen content of the atmosphere. Here, the atmosphere is assumed to have a mean surface temperature of 287.9 K, 0.06 bar of CO_2, with neither CH_4 nor O_2 nor O_3. Atmospheric water vapor is determined by self-consistent hydrological cycle modeling. Increasing N_2 increases the longwave forcing by enhancing pressure broadening of existing spectral lines. However, increasing N_2 also leads to a negative shortwave forcing by enhanced Rayleigh scattering. In total, the positive longwave forcing wins out, and climate warms. (Color graphics available online at www.liebertonline.com/ast)

As a primary result, our simulations generally agree with the predictions made by Goldblatt *et al.* (2009). With 2 PAL N_2, global mean surface temperatures increased by 5.0 K, reaching 292.9 K. With 3 PAL N_2, global mean surface temperatures increased by 9.7 K, reaching 297.6 K. Our 3 PAL N_2 simulation exhibited slightly more warming from increasing N_2 than was shown by Goldblatt *et al.* (2009). Differences are likely accounted for by the subtle positive cloud feedbacks found here and from magnified pressure broadening effects, as here we used 0.06 bar of CO_2 as a baseline case as opposed to 0.02 bar CO_2 and 10^{-4} bar CH_4 as a maximum used by Goldblatt *et al.* (2009).

4. Optimal Warming

For a second set of simulations, we combined the above-discussed warming mechanisms to construct optimal climate solutions for the duration of the Archean (3.8–2.5 Ga, corresponding to solar constants from 75% to 82% of the present day). We attempted to make realistic assumptions for the Archean climate system and then determined the atmospheric CO_2 needed to maintain modern-day global mean surface temperatures (~288 K).

We chose a rotation rate of 18 h per day for all simulations in this section. While Earth's rotation rate has varied continuously over time, the rate of despinning was slow during the Archean (Denis *et al.,* 2002). Regardless, the chosen rotation rate had only a minor effect on global climate compared with other influences discussed here (see Section 3.1). We assumed that CDNC were 20% of their present-day value (relative to the default settings in CAM3; see Table 3). This choice is consistent with estimates of CDNC if sea salt and dust are assumed to be the only available CCN for early Earth (Fan and Toon, 2011; Karydis *et al.,* 2011). This assumption yielded liquid cloud droplet effective radii of 13.7 μm over land and 23.9 μm over oceans and sea ice. Averaged globally, liquid cloud droplet effective radii are 19.1 μm in the lower troposphere. Note that this choice for the cloud droplet effective radii is less than that postulated by Rosing *et al.* (2010) but is $\sim$2 μm greater than is observed in unproductive regions of the oceans today (Bréon *et al.,* 2002). We assumed land surface characteristics corresponding to dark bare soil on all land surfaces. Thus, we implicitly assumed that all emergent continents are dominated by basaltic rock. The albedo of dark bare soil is nearly indistinguishable from open ocean. Furthermore, replacing forested grid cells with bare soil (*i.e.,* desert) imparts a modest reduction to low-level clouds over land (see Section 3.2). We tested two separate atmospheric nitrogen inventories, corresponding to 1 PAL N_2 and then 2 PAL N_2. The 1 PAL N_2 case is safely within bounds set by geochemical indicators (Som *et al.,* 2012; Marty *et al.,* 2013). While 2 PAL N_2 is larger than their most probable values, it remains within the absolute upper limit postulated by Som *et al.* (2012) for 2.7 Ga and well within the theoretical limit given by Goldblatt *et al.* (2009). The time frame for the drawdown of atmospheric N_2 remains uncertain. However, logic would dictate that atmospheric N_2 inventories were likely to have been larger during the early Archean and smaller toward the end of the Archean. However, for simplicity here we kept N_2 constant at all times. We also included 10^{-4} bar of methane in our simulations. Photochemical ecosystem models predict that up to 0.035 bar of CH_4 could have been present in the anoxic early atmosphere (Kharecha *et al.,* 2005); thus 10^{-4} bar is a rather modest number. Atmospheric CH_4 would have been strongly modulated by the presence of early life and atmospheric chemistry; however, here it is a fixed parameter. The inclusion of 10^{-4} bar of methane can yield a $\sim$6 K increase in global mean surface temperature (Haqq-Misra *et al.,* 2008).

Optimal simulations benefit strongly from the combined effects of systematic warming mechanisms along with modest atmospheric CH_4. For the later Archean, optimal simulations have no trouble warming early Earth to global mean surface temperatures of 288 K well within constraints on paleoatmospheric CO_2 (Fig. 7). With 2 PAL N_2, at the end of the Archean (2.5 Ga, 82% solar constant), only 0.0024 bar of CO_2, about 6 PAL, is needed to maintain present-day surface temperatures. If we are limited to only 1 PAL N_2, still only 0.0048 bar of CO_2, about 12 PAL, is required at 2.5 Ga. Both solutions require CO_2 concentrations well below the uppermost limits proposed by Driese

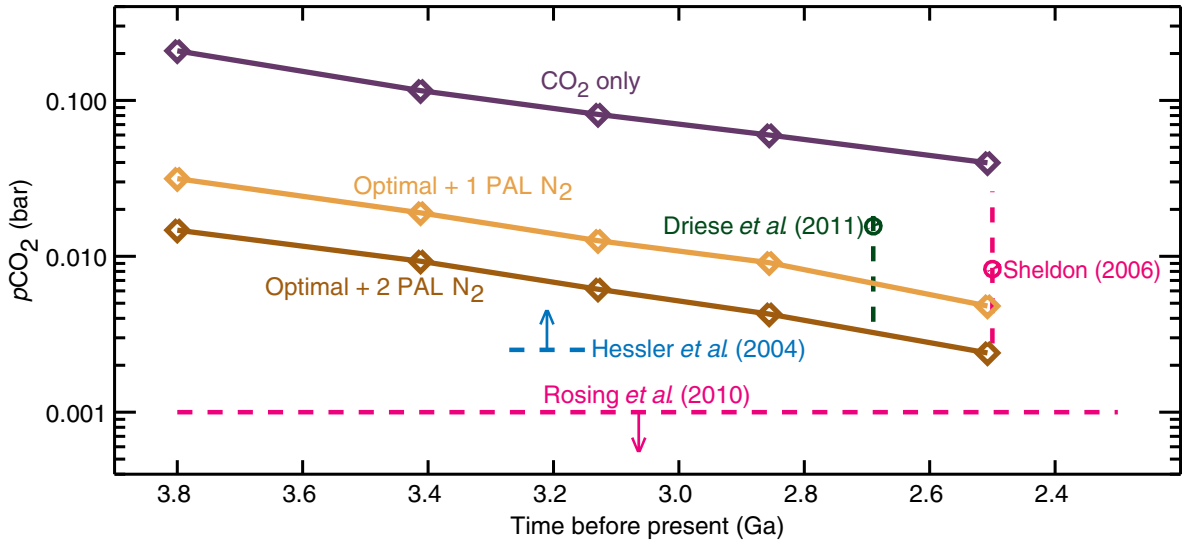

FIG. 7. Amount of carbon dioxide needed to maintain current global mean surface temperatures (288 K) over the course of the Archean. The dark line shows the amount of CO_2 needed if CO_2 alone is used to warm the Archean to present-day surface temperatures. Warmed by CO_2 only, current temperatures cannot be maintained within constraints given on CO_2 (marked on figure; Hessler *et al.,* 2004; Sheldon, 2006; Rosing *et al.,* 2010; Driese *et al.,* 2011). The orange and red lines show optimal warming solutions with 1 and 2 PAL N_2, respectively. Optimal warming solutions also include 10^{-4} bar of CH_4, an 18 h rotation rate, dark soil surface, and 20% CDNC. For 2 PAL of N_2, warm Archean solutions can be maintained throughout the Archean at CO_2 amounts below paleosol constraints on CO_2. Temperatures significantly warmer than 288 K could easily be achieved if CO_2 were raised up to the paleosol constraints ($\sim$0.01 to 0.02 bar CO_2) and if CH_4 were raised such that CH_4:$CO_2 \leq 0.1$. The CO_2 constraint given by Rosing *et al.* (2010) remains difficult to satisfy. (Color graphics available online at www.liebertpub.com/ast)

et al. (2011) and Sheldon (2006) of 0.018 bar and 0.025 bar, respectively, for the late Archean. At the beginning of the Archean (3.8 Ga, 75% solar constant), with 2 PAL N_2 and the warming mechanisms discussed above, present-day global mean surface temperatures can be maintained with only 0.0147 bar of CO_2, about 37 PAL. This again remains within the bounds on paleoatmospheric CO_2 defined by Driese *et al.* (2011) and Sheldon (2006). Thus, with 2 PAL N_2 we can maintain a warm Earth within paleosol constraints at all times of the Archean. However, with only 1 PAL N_2, 0.032 bar of CO_2, about 80 PAL, is needed to reach mean surface temperatures of 288 K at 3.8 Ga. This CO_2 concentration exceeds the uppermost limits derived from paleosols. However, CO_2 constraints are only defined for the later Archean, and it is generally believed that there may have been more atmospheric CO_2 during the early Archean as opposed to the late Archean. Conversely, solutions that rely only on a CO_2 greenhouse, with no CH_4 or additional warming mechanisms, cannot keep early Earth warm within proposed constraints on paleoatmospheric CO_2 at any time during the Archean.

The ratio of CH_4 to CO_2 remains less than 0.1 in all our optimal warming simulations. Thus, in all cases Titan-like photochemical hazes would not be expected to form (Domagal-Goldman *et al.,* 2008; Haqq-Misra *et al.,* 2008; Zerkle *et al.,* 2012); thus there is no need to incorporate their effects in this study. Hazes may have cooled Earth via the anti-greenhouse effect but may also have provided some benefits. A haze layer may have shielded early life-forms from harsh ultraviolet and may also have protected NH_3, a potent greenhouse gas, from photolysis (Sagan and Chyba, 1997; Wolf and Toon, 2010). With either 1 or 2 PAL N_2, the CO_2 required to reach present-day surface temperatures for the late Archean remains below paleosol-derived constraints. Thus, we could allowably increase both CO_2 and CH_4, warming the climate significantly above 288 K while still avoiding the issue of photochemical hazes.

CO_2 constraints for the early Archean remain unknown, as geochemical indicators primarily exist from the late Archean. It is conventionally believed that more CO_2 was in the atmosphere during the early Archean and then was slowly drawn down over time by the carbonate-silicate cycle. Given more lax constraints, one may suppose a case for the earliest Archean with 0.04 bar of CO_2 and 0.004 bar of CH_4 without significant haze formation. In such a case, for the earliest Archean (3.8 Ga, 75% solar constant), along with optimal warming assumptions given above, the global mean surface temperature reaches 307.5 K in our model, while the tropical sea surface temperatures reach 315 K. While these temperatures still fall short of those suggested by Knauth and Lowe (2003) and Robert and Chaussidon (2006), with the aid of non-greenhouse warming mechanisms ''hot'' Archean temperatures may be approached. Our study of hot Archean climates is limited as CAM3 encounters numerical instabilities when global mean surface temperatures push past ~313 K (Wolf and Toon, 2014).

Even under our optimal warming assumptions and 2 PAL N_2, present-day surface temperatures cannot be achieved near the CO_2 constraint of Rosing *et al.* (2010). While increased CH_4 could theoretically resolve this issue, large CH_4 concentrations would likely lead to the formation of thick photochemical hazes. Possibly other greenhouse gases such as NH_3, C_2H_6, or OCS could help rectify this discrepancy; however, they remain unproven. However, the plurality of CO_2 constraints place the upper limit well above that of Rosing *et al.* (2010). Hessler *et al.* (2004) placed a lower limit on CO_2 at 3.2 Ga at 0.0025 bar in direct contradiction to Rosing *et al.* (2010). The Rosing *et al.* (2010) constraint remains an outlier among geologically derived constraints on atmospheric CO_2. Some have argued that the methodology used by Rosing *et al.* (2010) is not robust (Dauphas and Kasting, 2011; Reinhard and Planavsky, 2011). Certainly, the debate on paleoatmospheric CO_2 will continue as new measurements come to light. At present, we find the Rosing *et al.* (2010) constraint on CO_2 to be too low to allow us to resolve the faint young Sun paradox.

5. Conclusion

In this study, we examined systematic changes to Earth's rotation rate, surface albedo, cloud properties, and atmospheric nitrogen content in hopes of incorporating non-greenhouse means of warming early Earth. While the overall effect of an increased rotation rate is slight, assumptions of darker land surface albedos, reduced CCN, and increased atmospheric N_2 all yield modest global mean surface temperature increases, from 3 to 7 K each given plausible assumptions. One can argue convincingly for the validity of the above-discussed warming mechanisms; however, they remain difficult to explicitly prove through the geological record. While no one mechanism provides a singular solution to the faint young Sun paradox, an aggregate solution that incorporates modest CH_4 concentrations along with the discussed warming mechanisms can resolve the faint young Sun paradox for all times of the Archean without violating constraints on CO_2 derived from paleosols. Hot Archean temperatures may even be possible. Combining lowered expectations for Archean seawater temperatures (Jaffrés *et al.,* 2007; Hren *et al.,* 2009; Blake *et al.,* 2010), relatively lenient atmospheric CO_2 constraints (Sheldon, 2006; Driese *et al.,* 2011), wide uncertainties on atmospheric CH_4 concentrations (Kharecha *et al.,* 2005), and numerous additional mechanisms for providing surface warming (Goldblatt *et al.,* 2009; Rosing *et al.,* 2010), there may be numerous permutations for resolving the faint young Sun paradox. Recent results from numerous different general circulation models indicate that sufficiently warming early Earth does not now appear to be a problem (Charnay *et al.,* 2013; Kunze *et al.,* 2013; Wolf and Toon, 2013). Intercomparison of models remains an important tool for gaining confidence in our theoretical results. However, the precise combination of solar constant, surface temperature, CO_2, CH_4, N_2, and other effects may remain difficult to pin down precisely without better geological constraints.

Acknowledgments

We thank NASA Earth and Space Science Fellowship award NNX10AR97H and NASA Exobiology award NNX10AR17G for financial support. This work utilized the Janus supercomputer, which is supported by the National Science Foundation (award number CNS-0821794) and the University of Colorado at Boulder. We thank J.F. Kasting and an anonymous reviewer for helpful comments on this manuscript.

Abbreviations

CAM3, Community Atmospheric Model version 3.0; CCN, cloud condensation nuclei; CDNC, cloud droplet number concentration; PAL, present atmospheric level.

References

Andreae, M.O. (2007) Aerosols before pollution. *Science* 315: 50–51.

Blake, R.E., Chang, S.J., and Lepland, A. (2010) Phosphate oxygen isotopic evidence for a temperate and abiologically active Archaean ocean. *Nature* 464:1029–1033.

Bony, S., Colman, R., Kattsov, V.M., Allan, R.P., Bretherton, C.S., Dufresne, J.L., Hall, A., Hallegate, S., Holland, M.M., Ingram, W., Randall, D.A., Soden, B.J., Tselioudis, G., and Wedd, M.J. (2006) How well do we understand and evaluate climate change feedback processes? *J Clim* 19:3445–3482.

Bréon, F.-M., Tanré, D., and Genersos, S. (2002) Aerosol effect on cloud droplet size monitored from satellite. *Science* 295: 834–838.

Caballero, R. and Huber, M. (2013) State-dependent climate sensitivity in past warm climates and its implications for future climate. *Proc Natl Acad Sci USA* 110:14162–14167.

Charnay, B., Forget, F., Wordsworth, R., Leconte, J., Millour, E., Codron, F., and Spiga, A. (2013) Exploring the faint young Sun problem and possible climates of the Archean Earth with a 3-D GCM. *J Geophys Res Atmospheres* 118: 10414–10431.

Chen, C. and Cotton, W.R. (1987) The physics of the marine stratocumulus-capped mixed layer. *Journal of the Atmospheric Sciences* 44:2951–2977.

Collins, W.D., Rasch, P.J., Boville, B.A., Hack, J.J., McCaa, J.R., Williamson, D.L., Kiehl, J.T., Briegleb, B., Bitz, C., Lin, S.-J., Zhang, M., and Dai, Y. (2004) *Description of the NCAR Community Atmosphere Model (CAM 3.0),* NCAR Technical Note/TN-464 + STR, National Center for Atmospheric Research, Boulder, CO. Available online at http://www.cesm.ucar.edu/models/atm-cam/docs/description/description.pdf.

Collins, W.D., Rasch, P.J., Boville, B.A., Hack, J.J., McCaa, J.R., Williamson, D.L., and Briegleb, B.P. (2006) The formulation and atmospheric simulation of the Community Atmosphere Model version 3 (CAM3). *J Clim* 19:2144–2161.

Dauphas, N. and Kasting, J.F. (2011) Low pCO_2 in the porewater, not in the Archean air. *Nature* 474, doi:10.1038/nature09960.

Denis, C., Schreider, A.A., Varga, P., and Zavoti, J. (2002) Despinning of the Earth rotation in the geological past and geomagnetic paleointensities. *Journal of Geodynamics* 34: 667–685.

DeWitt, H.L., Trainer, M.G., Pavlov, A.A., Hasenkopf, C.A., Aiken, A.C., Jimenez, J.L., McKay, C.P., Toon, O.B., and Tolbert, M.A. (2009) Reduction in haze formation rate on prebiotic Earth in the presence of hydrogen. *Astrobiology* 9:447–453.

Dhuime, B., Hawkesworth, C.J., Cawood, P.A., and Storey, C.D. (2012) A change in the geodynamics of continental growth 3 billion years ago. *Science* 335:1334–1336.

Domagal-Goldman, S.D., Kasting, J.F., Johnston, D.T., and Farquhar, J. (2008) Organic haze, glaciations and multiple sulfur iostopes in the mid-Archean era. *Earth Planet Sci Lett* 269:29–40.

Driese, S.G., Jirsa, M.A., Ren, M., Brantley, S.L., Sheldon, N.D., Parker, D., and Schmitz, M. (2011) Neoarchean paleoweathering of tonalite and metabasalt: implications for reconstructions of 2.69 Ga early terrestrial ecosystems and paleoatmospheric chemistry. *Precambrian Res* 189:1–17.

Fan, T. and Toon, O.B. (2011) Modeling sea-salt aerosol in a coupled climate and sectional microphysical model: mass, optical depth and number concentration. *Atmos Chem Phys* 11:4587–4610.

Feulner, G. (2012) The faint young Sun problem. *Rev Geophys* 50, doi:10.1029/2011RG000375.

Goldblatt, C. and Zahnle, K.J. (2011) Clouds and the faint young Sun paradox. *Climate of the Past* 7:203–220.

Goldblatt, C., Claire, M.W., Lenton, T.M., Matthews, A.J., Watson, A.J., and Zahnle, K.J. (2009) Nitrogen-enhanced greenhouse warming on early Earth. *Nat Geosci* 2:891–896.

Gough, D.O. (1981) Solar interior structure and luminosity variations. *Solar Physics* 74:21–34.

Hansen, J., Sato, M., Ruedy, R., Nazarenko, L., Lacis, A., Schmidt, G.A., Russell, G., Aleinov, I., Bauer, M., Bell, N., Cairns, B., Canuto, V., Chandler, M., Cheng, Y., Del Genio, A., Faluvegi, G., Fleming, E., Friend, A., Hall, T., Jackman, C., Kelley, M., Kiang, N., Koch, D., Lean, J., Lerner, J., Lo, K., Menon, S., Miller, R., Minnis, P., Novakov, T., Oinas, V., Perlwitz, Ja., Perlwitz, Ju., Rind, D., Romanou, A., Shindell, D., Stone, P., Sun, S., Tausnev, N., Thresher, D., Wielicki, B., Wong, T., Yao, M., and Zhang, S. (2005) Efficacy of climate forcings. *J Geophys Res* 110, doi:10.1029/2005JD005776.

Haqq-Misra, J.D., Domagal-Goldman, S.D., Kasting, P.J., and Kasting, J.F. (2008) A revised, hazy methane greenhouse for the Archean Earth. *Astrobiology* 8:1127–1137.

Hegg, D.A., Covert, D.S., Johnson, H.H., and Woods, R.K. (2012) A simple relationship between cloud drop number concentration and precursor aerosol concentration for the regions of Earth's large marine stratocumulus decks. *Atmos Chem Phys* 12:1229–1238.

Hessler, A.M., Lowe, D.R., Jones, R.L., and Bird, D.K. (2004) A lower limit for atmospheric carbon dioxide levels 3.2 billion years ago. *Nature* 428:736–738.

Hren, M.T., Tice, M.M., and Chamberlain, C.P. (2009) Oxygen and hydrogen isotope evidence for a temperate climate 3.42 billion years ago. *Nature* 462:205–208.

Hunt, B.G. (1979) The influence of the Earth's rotation rate on the general circulation of the atmosphere. *Journal of the Atmospheric Sciences* 36:1392–1408.

Jaffrés, J.B.D., Shields, G.A., and Wallmann, K. (2007) The oxygen isotope evolution of seawater: a critical review of a long-standing controversy and an improved geological water cycle model for the past 3.4 billion years. *Earth-Science Reviews* 83:83–122.

Jenkins, G.S. (1996) A sensitivity study of changes in Earth's rotation rate with an atmospheric general circulation model. *Glob Planet Change* 11:141–154.

Jenkins, G.S. (2000) Global climate model high-obliquity solutions to the ancient climate puzzles of the faint young Sun paradox and low-altitude Proterozoic glaciation. *J Geophys Res* 106:7357–7370.

Jenkins, G.S. (2001) High-obliquity simulations for the Archean Earth: implications for climatic conditions on early Mars. *J Geophys Res* 106:32903–32913.

Karydis, V.A., Kumar, P., Barahona, D., Sokolik, I.N., and Nenes, A. (2011) On the effect of dust particles on global cloud condensation nuclei and cloud droplet number. *J Geophys Res* 116, doi:10.1029/2011JD016283.

Kharecha, P., Kasting, J., and Siefert, J. (2005) A coupled atmosphere-ecosystem model of the early Archean Earth. *Geobiology* 3:53–76.

Kienert, H., Feulner, G., and Petoukhov, V. (2012) Faint young Sun problem more severe due to ice-albedo feedback and higher rotation rate of the early Earth. *Geophys Res Lett* 39, doi:10.1029/2012GL054381.

Knauth, L.P. and Lowe, D.R. (2003) High Archean climatic temperature inferred from oxygen isotope geochemistry of cherts in the 3.5 Ga Swaziland Supergroup, South Africa. *Geol Soc Am Bull* 115:566–580.

Kristjánsson, J.E. and Kristiansen, J. (2000) Impact of a new scheme for optical properties of ice crystals on climates of two GCMs. *J Geophys Res* 105:10063–10079.

Kump, L.R. and Pollard, D. (2008) Amplification of cretaceous warmth by biological cloud feedbacks. *Science* 320:195.

Kunze, M., Godolt, M., Langematz, U., Grenfell, J.L., Hamann-Reinus, A., and Rauer, H. (2013) Investigating the early Earth faint young Sun problem with a general circulation model. *Planet Space Sci,* http://dx/doi.org/10.1016/j.pss.2013.09.11.

Le Hir, G., Teitler, Y., Fluteau, F., Donnadieu, Y., and Philippot, P. (2013) The faint young Sun problem revisited with a 3-D climate-carbon model—Part 1. *Climate of the Past* 9:1509–1534.

Marty, B., Zimmermann, L., Pujol, M., Burgess, R., and Philippot, P. (2013) Nitrogen isotopic composition and density of the Archean atmosphere. *Science* 342:101–104.

Navarra, A. and Boccaletti, G. (2002) Numerical general circulation experiments of sensitivity to Earth rotation rate. *Climate Dynamics* 19:467–483.

Rasch, P.J. and Kristjánsson, J.E. (1998) A comparison of the CCM3 model climate using diagnosed and predicted condensate parameterizations. *J Clim* 11:1587–1614.

Reinhard, C.T. and Planavsky, N.J. (2011) Mineralogical constraints on Precambrian pCO_2. *Nature* 474, doi:10.1038/nature09959.

Robert, F. and Chaussidon, M. (2006) A paleotemperature curve for the Precambrian oceans based on silicon isotopes in cherts. *Nature* 443:969–972.

Rondanelli, R. and Lindzen, R.S. (2010) Can thin cirrus clouds in the tropics provide a solution to the faint young Sun paradox? *J Geophys Res* 115, doi:10.1029/2009JD012050.

Rosing, M.T., Bird, D.K, Sleep, N.H., and Bjerrum, C.J. (2010) No climate paradox under the faint early Sun. *Nature* 464: 744–749.

Rossow, W.B., Henderson-Sellers, A., and Weinreich, S.K. (1982) Cloud feedback: a stabilizing effect for the early Earth. *Science* 217:1245–1247.

Rye, R., Kuo, P.H., and Holland, H.D. (1995) Atmospheric carbon dioxide concentrations before 2.2 billion years ago. *Nature* 378:603–605.

Sagan, C. and Chyba, C. (1997) The early faint Sun paradox: organic shielding of ultraviolet-labile greenhouse gases. *Science* 276:1217–1221.

Sagan, C. and Mullen, G. (1972) Evolution of atmospheres and surface temperatures. *Science* 276:52–56.

Schopf, J.W. (2006) Fossil evidence of Archaean life. *Philos Trans R Soc Lond B Biol Sci* 361:869–885.

Sheldon, N.D. (2006) Precambrian paleosols and atmospheric CO_2 levels. *Precambrian Res* 147:148–155.

Shields, G.A. and Kasting, J.F. (2007) Evidence for hot early oceans? *Nature* 447:E1–E2.

Som, S.M., Catling, D.C., Harnmeijer, J.P., Polivka, P.M., and Buick, R. (2012) Air density 2.7 billion years ago limited to less than twice modern levels by fossil raindrop imprints. *Nature* 484:359–362.

Urata, R.A. and Toon, O.B. (2013) Simulations of the martian hydrologic cycle with a general circulation model: implications for the ancient martian climate. *Icarus* 226:229–250.

Williams, G.E. (2000) Geological constraints on the Precambrian history of Earth's rotation and the Moon's orbit. *Rev Geophys* 38:37–59.

Wolf, E.T. and Toon, O.B. (2010) Fractal organic hazes provided an ultraviolet shield for Early Earth. *Science* 328: 1266–1268.

Wolf, E.T. and Toon, O.B. (2013) Hospitable Archean climates simualted by a general circulation model. *Astrobiology* 13: 1–19.

Wolf, E.T. and Toon, O.B. (2014) Delayed onset of runaway and moist greenhouse climate for Earth. *Geophys Res Lett* 41, doi:10.1002/2013GL058376.

Zahnle, K. and Walker, J.C.G. (1987) A constant daylength during the Precambrian era? *Precambrian Res* 37:95–105.

Zerkle, A.L., Claire, M.W., Domagal-Goldman, S.D., Farquhar, J., and Poulton, S.W. (2012) A bistable organic-rich atmosphere on the Neoarchaean Earth. *Nat Geosci* 5:359–363.

Zhang, M., Lin, W., Bretherton, C.S., Hack, J.J., and Rasch P.J. (2003) A modified formulation of fractional stratiform condensation rate in the NCAR Community Atmospheric Model CAM2. *J Geophys Res* 108, doi:10.1029/2002JD002523.

Address correspondence to:
Eric Wolf
Laboratory for Atmospheric and Space Physics
3665 Discovery Drive
Campus Box 600
University of Colorado
Boulder, CO 80303-7820

E-mail: eric.wolf@colorado.edu

Submitted 25 October 2013
Accepted 28 January 2014